

## Electronic Supplementary Information

# Diffusion controlled porous WO<sub>3</sub> thin film photoanodes for efficient solar-driven photoelectrochemical permanganic acid production

Tomohiko Nakajima,<sup>\*a</sup> Megumi Kanaori,<sup>a</sup> Hiroyuki Tateno,<sup>b</sup> Junichi Nomoto,<sup>a</sup> Yugo Miseki,<sup>b</sup> Tetsuo Tsuchiya<sup>a</sup> and Kazuhiro Sayama<sup>b</sup>

<sup>a</sup> Advanced Coating Technology Research Center, National Institute of Advanced Industrial Science and Technology, Tsukuba Central 5, 1-1-1 Higashi, Tsukuba, Ibaraki 305-8565, Japan.

<sup>b</sup> Research Center for Photovoltaics, National Institute of Advanced Industrial Science and Technology, Tsukuba Central 5, 1-1-1 Higashi, Tsukuba, Ibaraki 305-8565, Japan.

### Phase purity and crystal structure of the porous WO<sub>3</sub> thin film photoanode

The XRD pattern of WO<sub>3</sub> thin film prepared on the FTO substrate was shown in Fig. S1. The multiple diffraction peaks at around 22.5–25.0° were evaluated to be 3 peaks indicating a monoclinic  $P2_1/c$  space group, and the 200 peak was very intense. All of the reflection positions were almost consistent with the reported values (JCPDS 20-1324<sup>1</sup>). Based on this analysis, we concluded that the obtained WO<sub>3</sub> thin film can be assigned to be a pure  $\gamma$ -phase of WO<sub>3</sub> with the preferential 100 orientation.

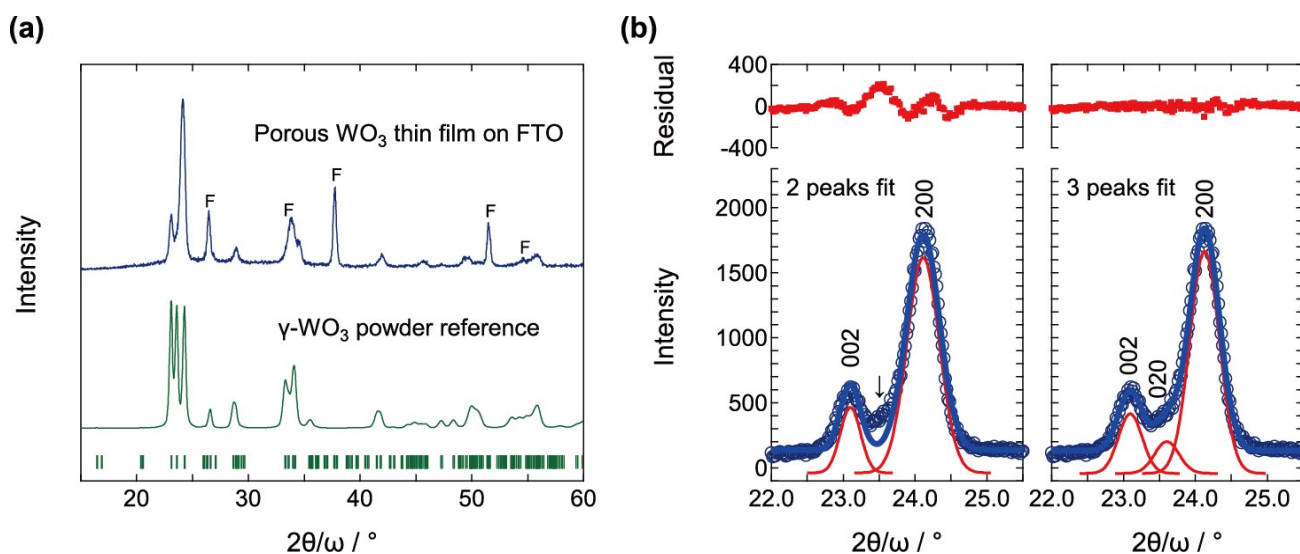


**Fig. S1:** (a) XRD patterns of the WO<sub>3</sub> thin film photoanode and the  $\gamma$ -WO<sub>3</sub> powder. The F represents the peaks assigned to the FTO. (b) The diffraction pattern for the WO<sub>3</sub> thin film was fitted as 2 and 3 peaks at around 22.5–25.0°. The multiple peak deconvolution analysis revealed that the 3 peak fitting associated with the monoclinic space group was very reasonable.

### PEC measurement setup and spectrum of illuminated solar simulator

The simulated sunlight at 1 Sun was illuminated from the backside of WO<sub>3</sub> film photoanode to avoid the excess absorption of illuminated light by the colored electrolytes contained Mn ions.

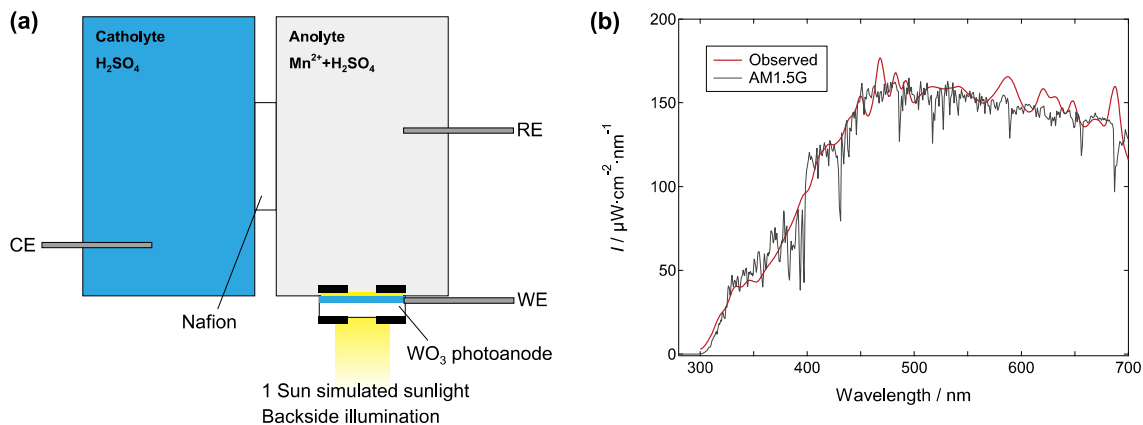


**Fig. S2:** (a) The experimental setup for PEC measurements. (b) The spectra for  $100 \text{ mW}\cdot\text{cm}^{-2}$  AM1.5G (1 SUN) and simulated solar light from a 150 W Xe lamp (XES-40S2-CE, San-Ei Electric)

### Determination of $\text{Mn}^{7+}$ and $\text{S}_2\text{O}_8^{2-}$ quantity in the solutions

The production of  $\text{MnO}_4^-$  ions ( $\text{Mn}^{7+}$ ) was evaluated by colorimetry by using the UV-VIS spectroscopy. Firstly, the absorption spectra of reference solutions for  $\text{Mn}^{2+}$  ( $\text{MnSO}_4$ ) and  $\text{Mn}^{7+}$  ( $\text{KMnO}_4$ ) in the aqueous sulfuric acid were measured (Fig. S3), and we confirmed that the  $\text{Mn}^{2+}$  was transparent in the range of 400–800 nm, and the spectral shape was almost unchanged in each sulfuric acid concentration and the intensity was just varied by the Mn ion concentrations. By using the reference  $\text{KMnO}_4$  spectra, the  $\text{MnO}_4^-$  ions ( $\text{Mn}^{7+}$ ) concentration was determined by the absorption peak intensity at 545 nm. The colorimetry for quantitative analysis of the  $\text{MnO}_4^-$  ions ( $\text{Mn}^{7+}$ ) concentration is a very reliable way in this study, since the other methods such as an observation of oxidation of reactants by the evolved  $\text{Mn}^{7+}$  would have a possibility that the reaction is affected by other high valence manganese ions. The production of  $\text{S}_2\text{O}_8^{2-}$  was also evaluated by colorimetry. After the consumption of  $\text{Mn}^{7+}$  by the successive reaction with the  $\text{Mn}^{2+}$  residue, the obtained solution specimen was mixed with equivalent amount of 0.01 M  $\text{FeSO}_4$  and 1 M  $\text{H}_2\text{SO}_4$  solution. The optical absorbance spectra were measured after the stirring of mixed solutions, and the  $\text{S}_2\text{O}_8^{2-}$  quantity was evaluated from the absorption at 310 nm.

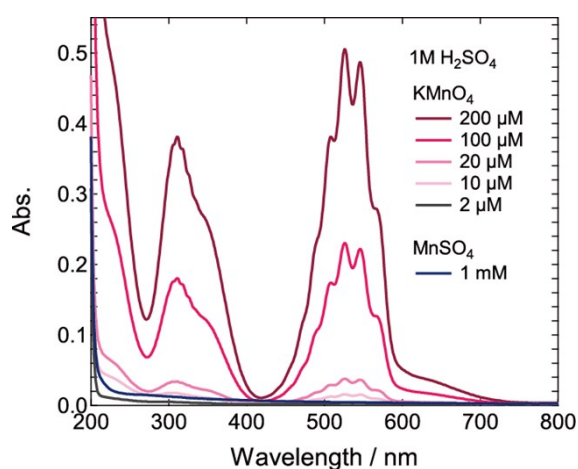


**Fig. S3:** The absorption spectra for the reference solutions of  $\text{KMnO}_4$  and  $\text{MnSO}_4$  in 1.0 M  $\text{H}_2\text{SO}_4$  solution.

### Thickness and morphological effect of WO<sub>3</sub> photoanodes on the PEC property

We prepared WO<sub>3</sub> film photoanodes by several processes to check the film thickness and morphology effects on the PEC property. In the nanoparticle dispersion coating process,<sup>2</sup> the obtained films have 1–7 μm of thickness and nanopores in the layer (Fig. S5a). Additionally, to vary the porosity we prepared samples by using dispersions with and without polyethylene glycol (PEG) 300 and by the inter-particle necking which was carried out by a 2-step coating (0.3 M tungsten phenoxide solution was deposited after the coating of nanoparticle dispersion). The solution deposition means the preparation process described in the main text. To vary the morphology, we also prepared by the samples without the addition of ethylcellulose, resulting in the dense films (Fig. S5b). The samples obtained by anodization process which was carried out by using W metal in H<sub>3</sub>PO<sub>4</sub> electrolyte at 100 °C under 8 V of bias voltage, the dense oxide layer was found under the anodized layer. We compared the PEC properties for the obtained samples, and found a clear tendency: porous thick films gave the large photocurrent density while the  $\eta(\text{Mn}^{7+})$  was reduced with the increasing thickness. On the contrary, the photocurrent density was not high in the thin films, however, the  $\eta(\text{Mn}^{7+})$  was enhanced. Less porosity of layer was favorable to obtain the  $\eta(\text{Mn}^{7+})$ , linking to the degradation of film surface by the successive reaction of Mn<sup>7+</sup> with the Mn<sup>2+</sup> residue described in the main text. On the basis of these results, we employed three WO<sub>3</sub> film photoanodes as the main and reference samples, which are expressed as the red and blue colored bars in Fig. S4. The detailed preparation procedures for pn-, dn-, pk-, pk2- and an-WO<sub>3</sub> photoanodes are summarized in Table S1.

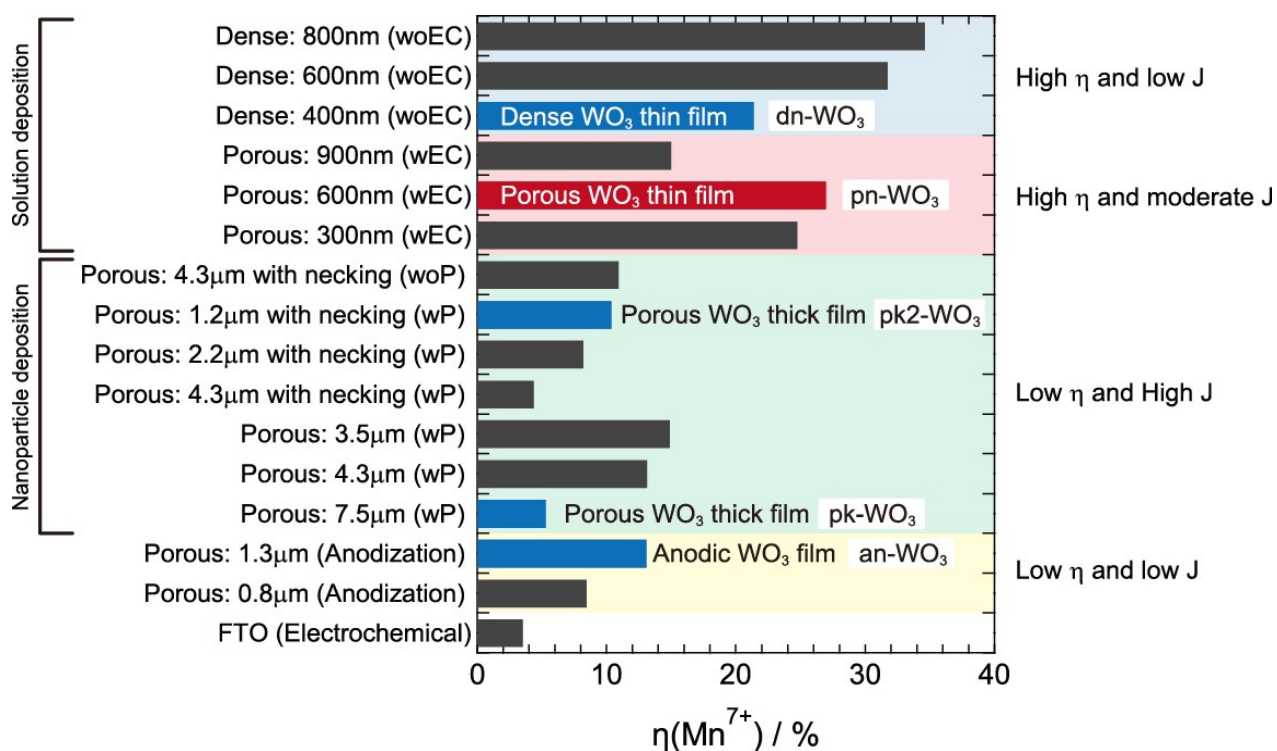
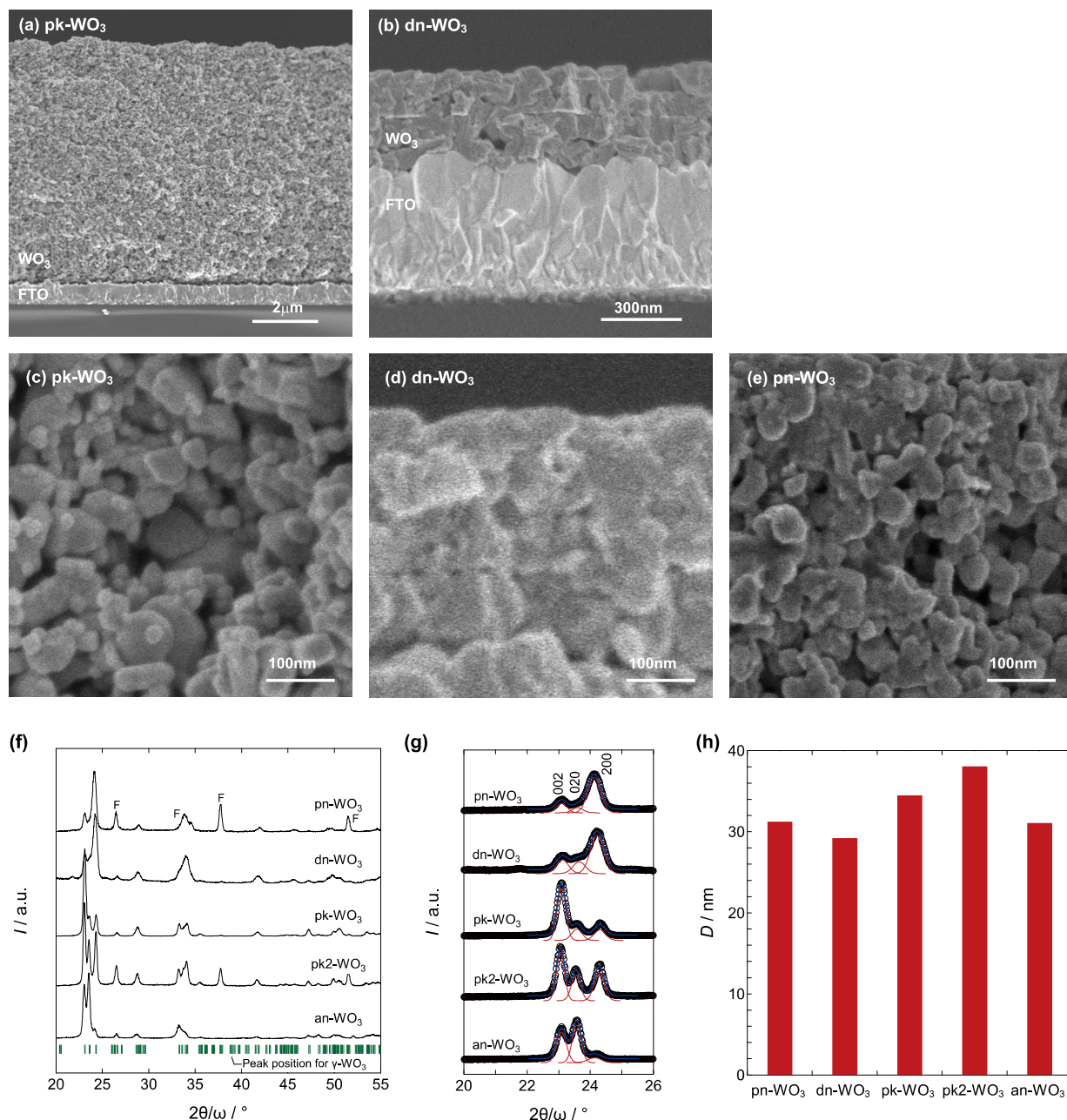


**Fig. S4:** The preparation process and thickness dependences of  $\eta(\text{Mn}^{7+})$  for the WO<sub>3</sub> film photoanodes in 1.0 mM MnSO<sub>4</sub> and 1.0 M H<sub>2</sub>SO<sub>4</sub> electrolyte at 1.3 V<sub>RHE</sub> for 1 h. The wP, woP, wEC and woEC represent the solution/dispersion “with PEG300”, “without PEG300”, “with ethylcellulose” and “without ethylcellulose”, respectively. The colored bars indicate the samples which are introduced in the main text as pn-, pk-, pk2-, an- and dn-WO<sub>3</sub> photoanodes.

**Table S1** Sample preparation conditions

Photoanode	Process	Procedure
pn-WO <sub>3</sub>	Solution deposition	A volume of 2.0 mL of 0.3 M tungsten phenoxide in toluene was mixed with 0.05 g of ethylcellulose, and the resulting solution was spin coated at 1000 rpm for 15 s onto FTO glass substrate. The film produced was preheated at 500 °C for 5 min. The coating and preheating processes were repeated four times, and the preheated film was then fired at 550 °C for 60 min in air.
dn-WO <sub>3</sub>	Solution deposition	0.3 M tungsten phenoxide in toluene was spin coated at 1000 rpm for 15 s onto FTO glass substrate. The film produced was preheated at 500 °C for 5 min. The coating and preheating processes were repeated four times, and the preheated film was then fired at 550 °C for 60 min in air.
pk-WO <sub>3</sub>	Nanoparticle deposition	WO <sub>3</sub> nanocrystal powder was ball milled in isopropanol for 6 h with a toluene solution of tungsten phenoxide. PEG300 was added to the WO <sub>3</sub> dispersion in a 1:1 volume ratio. The WO <sub>3</sub> dispersion was spin coated at 2000 rpm for 10 s onto FTO glass substrate. The film was preheated at 500 °C for 5 min. The coating and preheating processes were repeated 13 times, and the preheated film was then fired at 550 °C for 30 min in air.
pk2-WO <sub>3</sub>	Nanoparticle deposition	The same WO <sub>3</sub> dispersion for the pk-WO <sub>3</sub> was spin coated at 2000 rpm for 10 s onto FTO glass substrates. The film was preheated at 500 °C for 5 min. The coating and preheating processes were repeated 2 times. 0.3 M tungsten phenoxide solution was additionally spin coated at 1000 rpm for 15 s. The film was preheated at 500 °C for 5 min, and then was finally fired at 550 °C for 60 min in air.
an-WO <sub>3</sub>	Anodization	The anodization process was carried out by using W metal in H <sub>3</sub> PO <sub>4</sub> electrolyte at 100 °C under 8 V of bias voltage for 120 min. The obtained precursor was fired at 550 °C for 30 min in air.

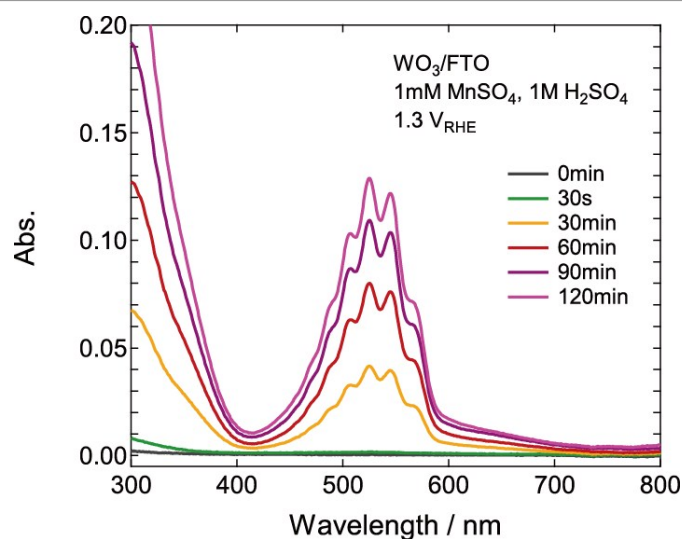
Figure S5f shows the xrd patterns for the pn-, dn-, pk-, pk2- and an-WO<sub>3</sub> photoanodes. The crystal orientation property along the substrate normal was different from each other, however, the crystallites/crystal grains in the WO<sub>3</sub> nanostructures had contact with the electrolyte in random crystal face directions as shown in Figs. 7 and S5a-e. Moreover, the calculated crystallite size for the all photoanodes was 29–38 nm, indicating the very similar crystallinity. (The crystallite size was evaluated by using Scherrer's equation,  $D = (K \cdot \lambda / \beta \cos \theta)$ , where  $K$  is the Scherrer constant ( $K = 0.94$ ),  $\lambda$  is the wavelength of the incident X-ray ( $\lambda = 0.15401$  nm),  $\beta$  is the full width at half-maximum intensity of the 002 peak, and  $\theta$  is the Bragg diffraction angle for the 002 reflection.) These results suggest that the crystal property among the tested photoanodes would not have a considerable effect on the PEC property.



**Fig. S5:** Cross-sectional views of FESEM images for reference WO<sub>3</sub> photoanodes; (a) the pk-WO<sub>3</sub> and (b) the dn-WO<sub>3</sub>. The enlarged view of grain morphology for (c) the pk-WO<sub>3</sub>, (d) the dn-WO<sub>3</sub> and (e) the pn-WO<sub>3</sub>. (f) XRD patterns and (g) peak fittings for all WO<sub>3</sub> film photoanodes. The F represents the peaks assigned to the FTO substrate. (h) The calculated crystallite size for the WO<sub>3</sub> thin film photoanodes.

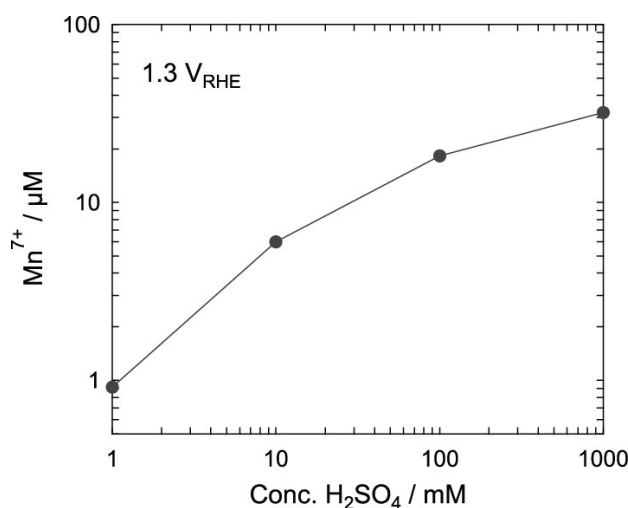
### The PEC property of pk-WO<sub>3</sub> photoanodes

Figure S6 shows the illumination time dependence of the PEC reaction in the electrolyte containing 1.0 mM Mn<sup>2+</sup> and 1.0 M H<sub>2</sub>SO<sub>4</sub> using the pk-WO<sub>3</sub> photoanode at 1.30 V<sub>RHE</sub>. As with the case of pn-WO<sub>3</sub> photoanodes (Fig. 3b), the chromatic change of the solution from colorless to pink during the illumination was observed (Fig. S6). The absorption peaks are also assigned to the MnO<sub>4</sub><sup>-</sup> ions (Mn<sup>7+</sup>). The evolved Mn<sup>7+</sup> for 30 min (4.8 C) at this PEC condition was 28 μM, and the η(Mn<sup>7+</sup>) was 5.2%.

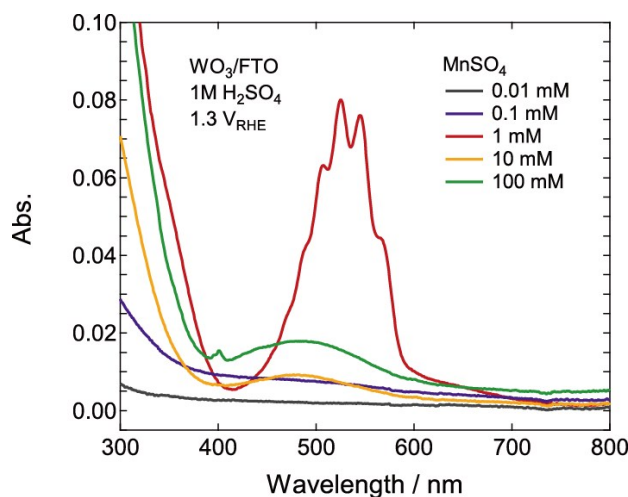


**Fig. S6:** Illumination-time dependence of absorption spectra for the pk-WO<sub>3</sub> photoanode in the electrolyte containing 1.0 mM Mn<sup>2+</sup> and 1.0 M H<sub>2</sub>SO<sub>4</sub> under simulated sunlight at 1.3 V<sub>RHE</sub>.

The concentration dependences of Mn<sup>2+</sup> and H<sub>2</sub>SO<sub>4</sub> in the PEC reaction for the porous WO<sub>3</sub> thick film photoanode also showed similar behavior with the porous thin film photoanodes (Figs. S6–S8). The evolution of Mn<sup>7+</sup> increased with the increasing H<sub>2</sub>SO<sub>4</sub> concentration up to 1.0 M, and the Mn<sup>2+</sup> concentration dependence had a maximum at 1.0 mM. Above 10 mM of MnSO<sub>4</sub>, the broad absorption peak at 490 nm assigned to the Mn<sup>3+</sup> ions was also observed.

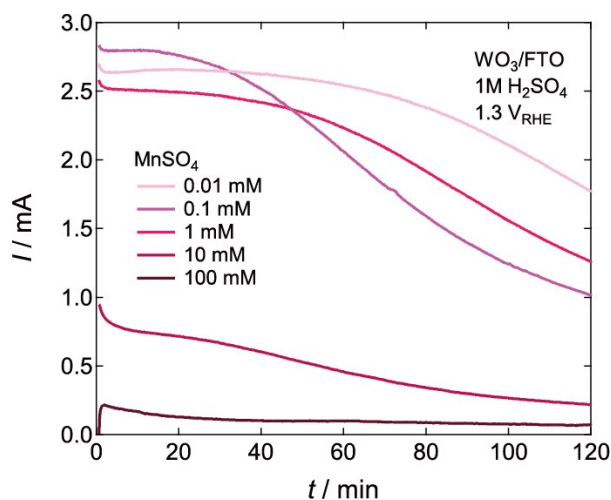


**Fig. S7:** H<sub>2</sub>SO<sub>4</sub> concentration dependence of the evolved Mn<sup>7+</sup> for the pk-WO<sub>3</sub> photoanode in the electrolyte containing 1.0 mM Mn<sup>2+</sup> under simulated sunlight at 1.3 V<sub>RHE</sub>.



**Fig. S8:**  $\text{MnSO}_4$  concentration dependence of absorption spectra for the pk- $\text{WO}_3$  photoanode in the electrolyte containing 1.0 M  $\text{H}_2\text{SO}_4$  under simulated sunlight at 1.3  $V_{\text{RHE}}$ .

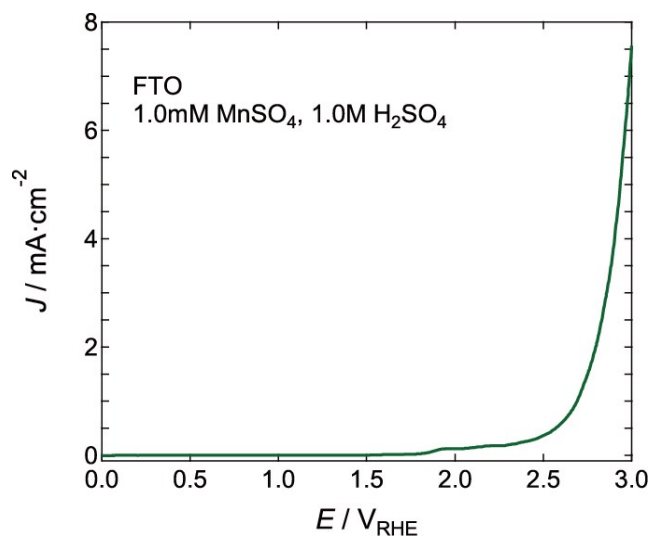
The  $\text{Mn}^{2+}$  concentration dependence of  $I$ - $t$  curves for the pk- $\text{WO}_3$  photoanode showed a gradual decrease of photocurrent (Fig. S9). Above 10 mM of  $\text{Mn}^{2+}$ , the photocurrent was very small from the initial state, and the thick brownish deposit was observed at the film surface.



**Fig. S9:** The  $\text{Mn}^{2+}$  concentration dependence of  $I$ - $t$  curves for the pk- $\text{WO}_3$  photoanode in 1.0 M  $\text{H}_2\text{SO}_4$  electrolyte at 1.3  $V_{\text{RHE}}$ .

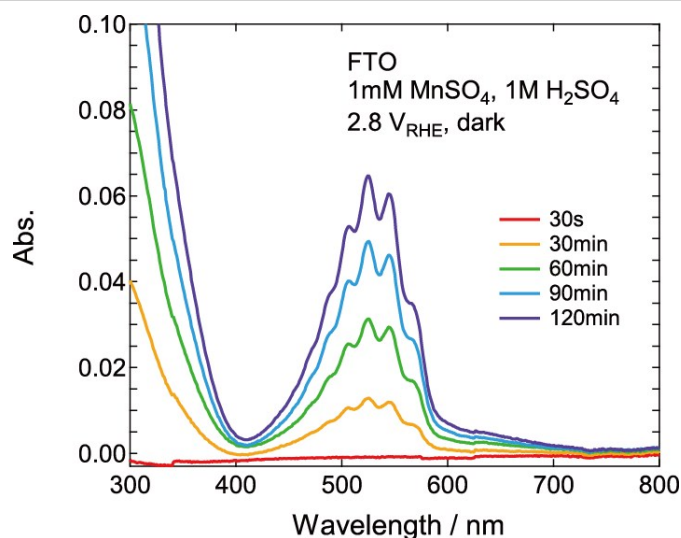
### The EC property of FTO anodes

Figure S10 shows the LSV curve for the electrolyte containing 1.0 mM  $\text{Mn}^{2+}$  and 1.0 M  $\text{H}_2\text{SO}_4$  ( $\text{pH} \approx 0.0$ ) using the FTO glass anode under the dark condition. The onset potential of the photocurrent was about 1.8  $V_{\text{RHE}}$ , and the  $J$  gradually increased up to 0.3  $\text{mA}\cdot\text{cm}^{-2}$  at 2.5  $V_{\text{RHE}}$ , followed by the rapid rise above 2.7  $V_{\text{RHE}}$ .



**Fig. S10:**  $J$ - $V$  curves for EC reaction in the FTO glass anode. The electrolyte was 1.0 mM  $\text{Mn}^{2+}$  and 1.0 M  $\text{H}_2\text{SO}_4$ .

Figure S11 shows the illumination time dependence of the PEC reaction in the electrolyte containing 1.0 mM  $\text{Mn}^{2+}$  and 1.0 M  $\text{H}_2\text{SO}_4$  using the FTO glass anode at 2.8  $V_{\text{RHE}}$ . The chromatic change of the solution from colorless to pink during the application of bias voltage was observed. The absorption peaks are assigned to the  $\text{MnO}_4^-$  ions ( $\text{Mn}^{7+}$ ) as well as the PEC reactions (Figs. 3b and S6). The evolved  $\text{Mn}^{7+}$  for 30 min (4.1 C) at this EC condition was 11  $\mu\text{M}$ , and the  $\eta(\text{Mn}^{7+})$  was 3.9%.



**Fig. S11:** Time dependence of absorption spectra for the FTO anode in the electrolyte containing 1.0 mM  $\text{Mn}^{2+}$  and 1.0 M  $\text{H}_2\text{SO}_4$  under dark condition at 2.8  $V_{\text{RHE}}$ .

### Dye absorption/desorption procedure

For the evaluation of surface area, we employed dye absorption/desorption experiments. Ru-based N719 dye (cis-bis (isothiocyanato) bis (2,2-bipyridyl 4,4-dicarboxylato) ruthenium (II) bis-tetrabutylammonium) was used. The obtained samples were immersed for 1 day at 40 °C in a mixture of acetonitrile and tert-butyl alcohol (1:1,v/v)

containing a 300mM N719 dye (Solaronix SA, Switzerland). After dye-absorption, the samples were rinsed acetonitrile to remove non-chemisorbed dye. Dye desorption measurements were carried out by immersing the samples in 5ml of 10mM KOH for 1 h followed by the concentration measurements by UV-VIS spectrometer at 520 nm. To confirm the reliability of the dye absorption analysis, we also carried out the Brunauer-Emmett-Teller (BET) surface-area measurements by N<sub>2</sub> adsorption-desorption at 77 K using a BELSORP-minill instrument (BEL Japan, Inc.) for the crystallized WO<sub>3</sub> polycrystalline powders. They were obtained by a combustion method using the same solution/dispersion and firing temperature with the pn- and pk-WO<sub>3</sub> (the original solution/dispersion was dried at 250 °C, and then fired at 550 °C for 60 min in air). The samples were degassed under a N<sub>2</sub> flow at 423 K for 60 min prior to data collection. Both of the dye-absorption method and the BET analysis showed similar tendency for the amount of surface absorption, therefore, we concluded that the dye absorption method was available to evaluate relative surface area analysis for the WO<sub>3</sub> film photoanodes.

**Table S2** Surface area analysis for the pn- and pk-WO<sub>3</sub>.

Photoanode	Dye absorption / mM·cm <sup>-3</sup> (Film)	BET surface area / m <sup>2</sup> ·g <sup>-1</sup> (Powder sample)
pn-WO <sub>3</sub>	75.3	27.5
pk-WO <sub>3</sub>	20.5	13.3

### **The PEC property of dn-, pk2 and an-WO<sub>3</sub> photoanodes**

Figure S12 shows the illumination time dependence of the PEC reaction in the electrolyte containing 1.0 mM Mn<sup>2+</sup> and 1.0 M H<sub>2</sub>SO<sub>4</sub> using the dn-, pk2 and an-WO<sub>3</sub> photoanodes at 1.30 V<sub>RHE</sub>. As with the case of pn- and pk-WO<sub>3</sub> photoanodes (Figs. 3b and S6), the chromatic change of the solution from colorless to pink during the illumination was observed. The absorption peaks are also assigned to the MnO<sub>4</sub><sup>-</sup> ions (Mn<sup>7+</sup>).

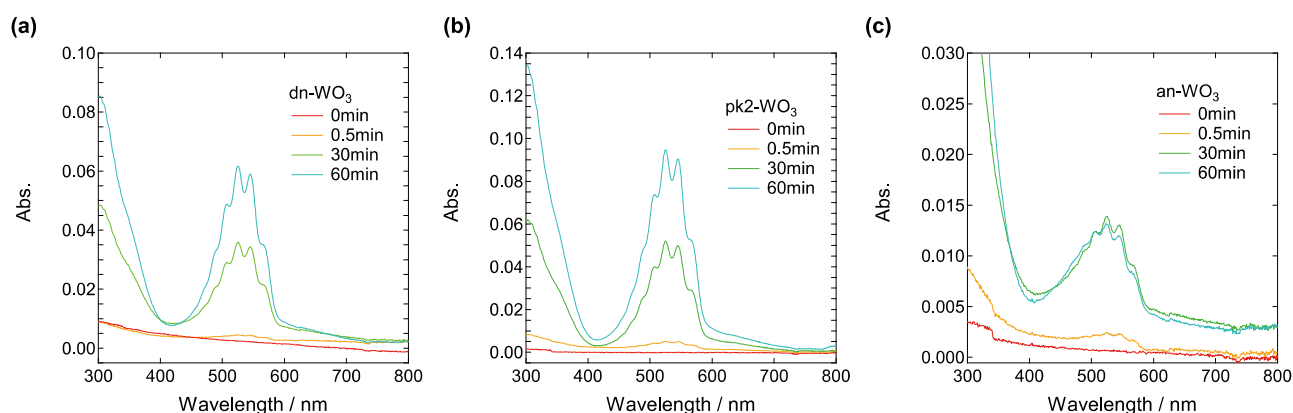


**Fig. S12:** Illumination-time dependence of absorption spectra for the dn-, pk2 and an-WO<sub>3</sub> photoanodes in the electrolyte containing 1.0 mM Mn<sup>2+</sup> and 1.0 M H<sub>2</sub>SO<sub>4</sub> under simulated sunlight at 1.3 V<sub>RHE</sub>.

### Effective diffusion coefficient ( $D_p$ )

The constrictivity  $\delta$  and tortuosity  $\tau$  for effective diffusion coefficient ( $D_p$ ) can be expressed as shown in Fig. S13.

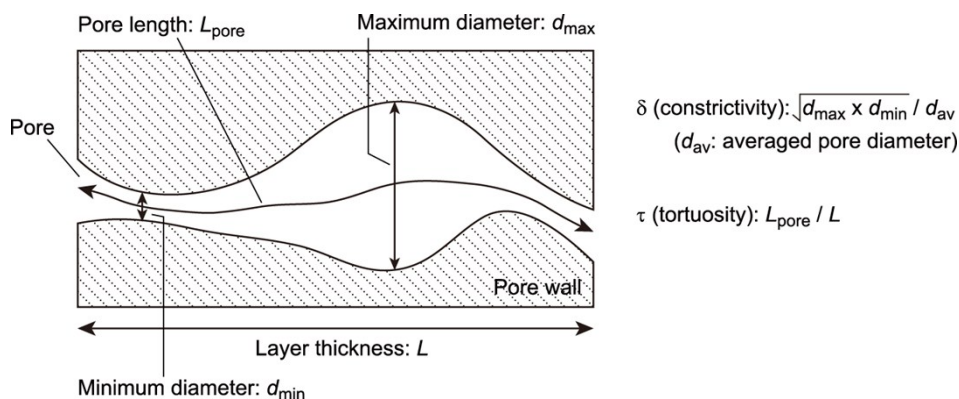


**Fig. S13:** Schematic illustration for the constrictivity and tortuosity.

### ABPE for the $\text{Mn}^{7+}$ production

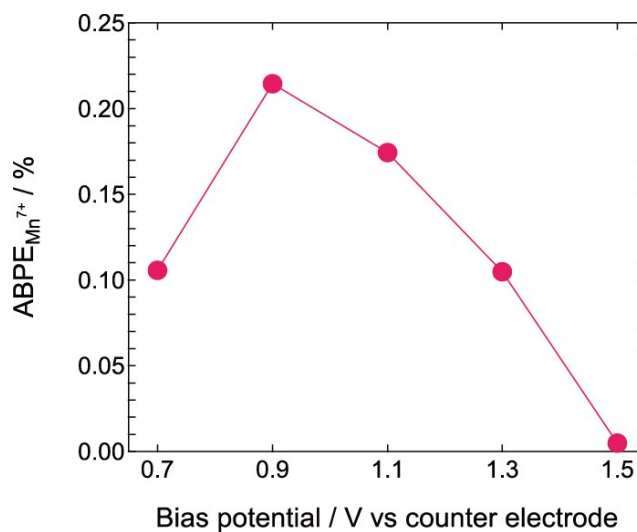


**Fig. S14:**  $ABPE_{\text{Mn}^{7+}}$  calculated for the evolution of  $\text{Mn}^{7+}$  in 1.0 mM  $\text{Mn}^{2+}$  and 1.0 M  $\text{H}_2\text{SO}_4$  electrolyte under the simulated solar light illumination. The  $ABPE_{\text{Mn}^{7+}}$  was calculated by using the faradaic efficiency at each applied bias voltage.

### Oxidation experiments: Quantitative evaluation of acetophenone

The production of acetophenone from ethylbenzene using the photoelectrochemically obtained  $\text{Mn}^{7+}$  ions was evaluated by colorimetry by using the UV-VIS spectroscopy. The absorption spectra of reference solutions for the acetophenone in ethylbenzene were measured. Both of ethylbenzene and acetophenone had an intense absorption below 280 nm, and only acetophenone showed two peaks at 290 and 320 nm (Fig. S15). The reference spectra were deconvoluted, and we used the absorption peak at 290 nm for the concentration analysis. Figure S15b shows the fitting result of absorption peaks for the reference solution of 2.0 mM

acetophenone in ethylbenzene. By the deconvolution of the absorption curves, we made a calibration curve by using the obtained absorption intensity at 290 nm at every concentration of acetophenone reference solutions (Fig. S15c).

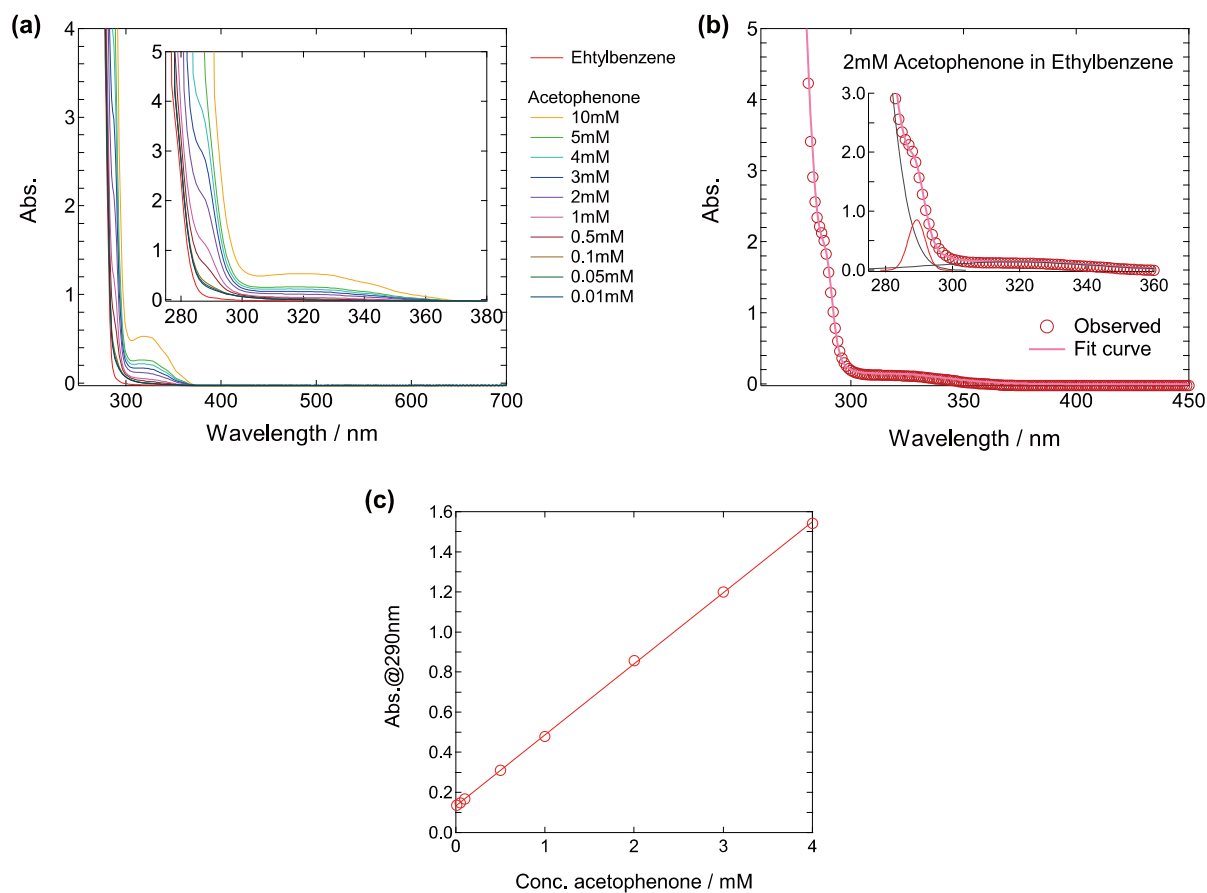


**Fig. S15:** (a) The absorption spectra for acetophenone in ethylbenzene and (b) the fitted spectral curve of reference 2.0 mM acetophenone solution. In the inset, three black and red lines represent the deconvoluted curves of raw data. (c) The peak intensity of deconvoluted curve at 290 nm as a function of acetophenone concentration in ethylbenzene.

## References

1. B. O. Loopstra and H. M. Rietveld, *J. Solid State Chem.*, 1991, **91**, 286.
2. T. Nakajima, A. Hagino, T. Nakamura, T. Tsuchiya and K. Sayama, *J. Mater. Chem. A*, 2016, **4**, 17809.